

The profile and equivalent width of the X-ray iron emission-line from a disk around a Kerr black hole

Y. Dabrowski¹, A.C. Fabian², K. Iwasawa², A.N. Lasenby¹, C.S. Reynolds^{2*}

1. Mullard Radio Astronomy Observatory, Cavendish Laboratory, Madingley Road, Cambridge CB3 0HE

2. Institute of Astronomy, Madingley Road, Cambridge CB3 0HA

26 August 2021

ABSTRACT

Recent X-ray observations have shown broad, skewed iron line emission from Seyfert 1 galaxies which is explained by the emission being fluorescence on a disk close to a black hole. During one interval, the line in MCG–6-30-15 was so broad and redshifted that a Kerr black hole is implied. We are therefore studying the effects of the Kerr metric on the line profile, and extending the work by Laor and Kojima which dealt only with extreme values of the spin parameter. Here we report that the spin parameter of the black hole in MCG–6-30-15 is high ($a/M > 0.94$), and invert the line profile to obtain the disk emissivity profile, which approximates a power-law. Continuum radiation returning to the disk because of the Kerr metric does not enhance the equivalent width of the line seen above 3 keV by more than about 20 per cent if the continuum source corotates with the disk.

Key words: accretion disks – black hole physics – line: profiles – X-rays: general

1 INTRODUCTION

X-ray observations of Seyfert 1 galaxies made with ASCA have shown that the iron emission lines discovered with GINGA (Pounds et al. 1990; Matsuoka et al. 1990) are broad (Fabian et al. 1994; Mushotzky et al. 1995; Reynolds 1997; Nandra et al. 1997). In particular, the line in MCG–6-30-15 was found to be both broad and skew from a 4.5 day long observation in 1994 (Tanaka et al. 1995). The line extends about 2 keV below the rest frame energy of the line (6.4 keV) and only 0.3 keV above. The line profile is well fitted by that expected from fluorescence of matter on the surface of an accretion disk less than 20 gravitational radii (i.e. $20r_g = 20GM/c^2$) from a black hole of mass M (Tanaka et al. 1995; Fabian et al. 1995). Much of the skewness of the line is explained by gravitational redshift, and is the first clear evidence for the effects of strong gravity.

Recent work examining variability in the line profile during the 4.5 day observation has revealed that it broadened still further during a deep minimum in the light curve (Iwasawa et al. 1996). The red (i.e. low energy) wing of the line extended further to the red and the blue (i.e. high energy) wing disappeared. This behaviour can be explained if much of the emission originates from within $6r_g$ (Iwasawa et al. 1996). Since a disk around a non-spinning, Schwarzschild

black hole does not extend within this region, it was concluded that the black hole must be spinning rapidly. In this case the Kerr metric applies and frame dragging causes the disk to extend inward of $6r_g$.

Light bending effects, in particular the return of some disk radiation to the disk itself, can then become significant (see e.g. Cunningham 1976). In Iwasawa et al. (1996) it was proposed (without detailed calculation) that these effects could enhance the strength (equivalent width) of the fluorescent line relative to the continuum, emitted above the disk, as required by the observations.

In this Letter we examine the line emission from a disk around a Kerr black hole, from the point of view of profile and of equivalent width, for the parameters relevant to MCG–6-30-15. Previously only the line profile of either a Schwarzschild black hole (Fabian et al. 1989) or a maximal Kerr black hole (Laor 1991; Kojima 1991) have been available for fitting. Here we explicitly fit for the angular momentum parameter of the black hole, as well as the inclination angle of the normal to the disk to the line of sight. In addition, results of a free-form fit to the radial emissivity profile of the disk in the fluorescent line are given, again for the first time.

* Present address: JILA, University of Colorado, Boulder, CO 80302, USA

2 DISKLINE MODEL USING THE KERR METRIC

The propagation of radiation from a disk around a Kerr black hole has already been studied (e.g. Cunningham 1975, 1976) and applied to model the observed profile of a line emission from the disk (Asaoka 1989; Kojima 1991; Laor 1991; Bromley, Chen & Miller 1997). The main parameters to which the spectra are sensitive are the inclination angle of the observer from the axis of symmetry i , the radial emissivity profile of the disk $\varepsilon(r)$ and the angular momentum parameter of the hole $a_* = a/M$, where a is the angular momentum and M is the black hole mass. (We note the model cannot discriminate a and M separately). We shall here investigate the effect of changes in i and a_* , and show a derived emissivity profile across the disk, at fixed i and a_* .

2.1 Assumptions and method of calculation

- The black hole belongs to the Kerr family of solutions. The metric used is in the Boyer–Lindquist form. The gravity of the disk itself (and of the clouds responsible for the fluorescence) is negligible.

- The accretion disk is assumed to be geometrically thin (i.e. thickness \ll smallest radius) and axially symmetric around the hole axis of rotation.

- The matter responsible for the fluorescent line is supposed to lie on the surface of the disk and rotates on equatorial circular geodesics. Emission starts at radius r_{in} , which is fixed to the radius of marginal stability r_{ms} (Novikov & Thorne 1973), up to an arbitrary outer radius r_{out} . No significant emission is expected far away from the centre since the line emissivity, described below, decreases rapidly (0.4% and 0.002% of its maximum for radii of $15r_g$ and $100r_g$ respectively if $a_* = 0.998$). Previous studies (Tanaka et al. 1995) suggest an outer radius of $\sim 10r_g$ – $16r_g$, so that we decided to fix this parameter to $r_{out} = 15r_g$. This constraint might have to be relaxed in future studies.

- Except for the case where we explicitly fit for the emissivity profile (see Section 3.1 below), then in the rest frame of the emitting material (which we usually call the *disk frame*), the emissivity of the fluorescent component $\varepsilon(r)$ [defined as energy emitted per unit proper time per unit proper area] is assumed to follow the law described in equation (11b) of Page & Thorne (1974). This law is derived for the continuum emission of the disk, but we suppose that the line flux (integrated across frequency in the emission rest frame) also follows this law. Since $\varepsilon(r)$ so defined vanishes at both r_{ms} and $r = \infty$, we expect this emissivity profile to be more realistic than a simple power law model (Fabian et al. 1989).

- We assume that the emitted fluorescent iron K_α line can be approximated by a δ -function in frequency, so that each emitted photon has an energy $h\nu_o$ of 6.40 keV in the disk frame (Iwasawa et al. 1996). The emission is assumed to be locally isotropic. Thus, in the disk frame, the emitted intensity $I_e(r, \nu_e)$ and flux $F_e(r, \nu_e)$ are described by:

$$F_e(r, \nu_e) = \pi I_e(r, \nu_e) = \varepsilon(r) \delta(\nu_e - \nu_o). \quad (1)$$

- The fluorescent photons are free to reach the observer unless they cross the hole event horizon (lost radiation) or they return to the disk itself. (See Section 4 and Cunningham 1976). The observer is assumed to be located in the

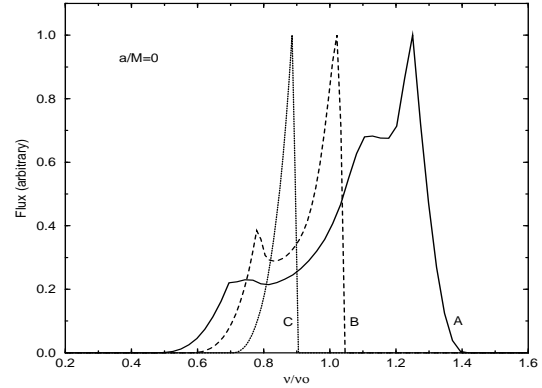


Figure 1. Predicted spectral line shapes for a Schwarzschild black hole ($a_* = 0$). A is for $i = 85^\circ$, B for $i = 30^\circ$, and C for $i = 0^\circ$.

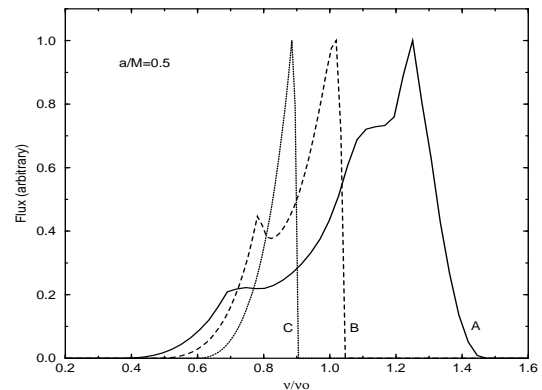


Figure 2. Same as Fig. 1 but for $a_* = 0.5$.

asymptotically flat region of space-time. In practice we use a distance of $1000r_g$.

The model then carries out a numerical integration of photon null geodesics backwards in time, from the observer to the disk, taking into account all the relativistic effects on both trajectories and redshift. The photons are emitted from the observer through a grid of equal solid angle pixels, which could be those of a CCD detector. At the end of the integration process, each image pixel is then associated with

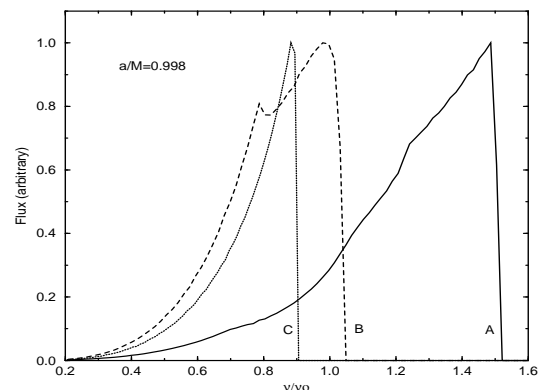


Figure 3. Same as for Fig. 1, but for $a_* = 0.998$, corresponding to an extreme Kerr black hole (Thorne, 1974).

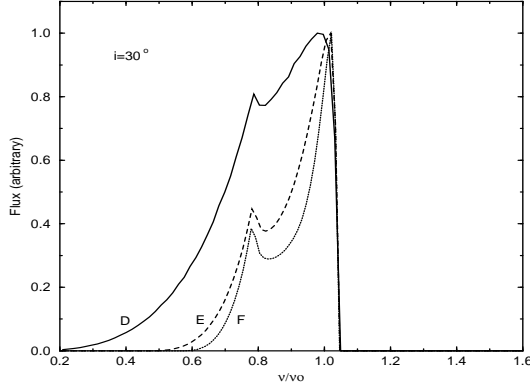


Figure 4. Predicted spectral line shapes at a fixed inclination $i = 30^\circ$. D is for an extreme Kerr black hole ($a_* = 0.998$), E for $a_* = 0.5$, and F for a Schwarzschild black hole ($a_* = 0$).

an emission radius r_e on the disk and a redshift z . We may compute the flux at the observer by using the phase space occupation number I_ν/ν^3 , which is invariant along the entire trajectory of the photon. Considering an interval ν to $\nu + \Delta\nu$ in observed frequency, then the observed flux in a pixel corresponding to solid angle $\Delta\Omega$ at the observer, will be

$$F(r_e, z) = \frac{\Delta\Omega}{\pi \Delta\nu} \frac{\varepsilon(r_e)}{(1+z)^4}, \quad (2)$$

if the interval $(\nu, \nu + \Delta\nu)$ contains $\nu_0/(1+z)$, and zero otherwise. Since redshift and flux are known for each pixel, images of those quantities can be plotted, such as those in Luminet (1979) or Bromley et al. (1997), but covering a wider range of parameters. Binning all $F(r_e, z)$ into the redshift axis, enables one to compute the observed line profile as seen by a distant observer.

2.2 The line profile as a function of spin parameter and inclination

Figs. 1, 2, 3 and 4 show predicted spectral lines over a range of a_* and i parameters and suggest that, for fixed emissivity profile, the overall line shape, in particular its width, is most sensitive to the inclination angle. For sufficiently high i (i.e. $i > 25^\circ$) the spectrum is double-peaked. The low redshift component is mainly due to the receding part of the disk from the observer and the high redshift photons essentially come from the approaching half-part, as shown below. In the case of more face-on inclinations (i.e. $i < 25^\circ$), the radial Doppler effect is not efficient enough and the observed line shape is a one-peak line with a weak blue component and a rather spread red contribution. Over the whole range of i , the red wing of the spectrum is being stretched by transverse Doppler and gravitational redshifts. This effect is boosted as the angular momentum a increases since the inner part of the disk then lies closer to the hole. Thus for a given i , the angular momentum controls the red wing extension (see Fig. 4). For a given a_* , i mainly constrains the upper limit of the blue part of the line (see Figs. 1, 2 and 3).

The radial Doppler shifts are illustrated in Fig. 5, where receding and approaching halves of the disk contributions are separated. An extreme black hole is used in Fig. 5 but with an emission area located between $r_{in} = 10r_g$ and $r_{out} =$

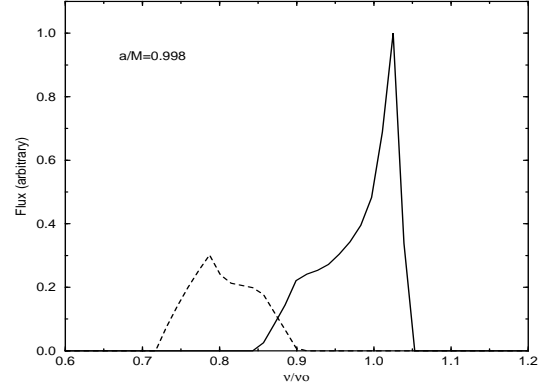


Figure 5. Contributions to the total lineshape from the receding (dashed) and approaching (solid) sections of the disk for $i = 30^\circ$, $a_* = 0.998$, $r_{in} = 10r_g$ and $r_{out} = 15r_g$.

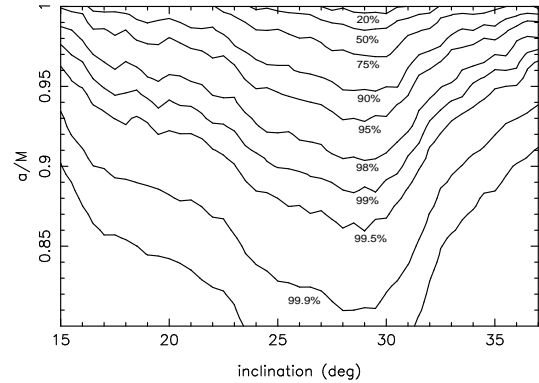


Figure 6. Contours of probability versus i and a_* are shown, calculated assuming a uniform prior on each parameter.

$15r_g$, in order to show a case where the two components are clearly separated in frequency. Such an appearance may be detectable if the X-ray emission is from a few localized flares which move around on the disk (see e.g. Iwasawa et al. 1996). Note the asymmetry of the two components, with the blue peak being much more intense than the red one. This blue boosting effect arises from the rather large redshift difference between the two halves.

3 FITS TO THE LINE PROFILES OF MCG-6-30-15

The evidence of strong gravity around a Kerr hole in MCG-6-30-15 has already been discussed in Iwasawa et al. (1996). This discussion included a comparison between the observed fluorescent K_α line at the period of lowest luminosity and a predicted Kerr lineshape corresponding to $i = 30^\circ$ and $a_* = 0.998$ (Laor 1991). We report here an actual fit using our diskline model in order to obtain joint constraints on both a_* and i . The data consist of 18 points lying between ~ 3 keV and ~ 8 keV and are described in detail in Iwasawa et al. (1996). We have carried out a χ^2 fit assuming the emissivity profile of Page & Thorne as discussed above. The results are presented in Figs. 6 and 7.

The χ^2 contours give relatively strong evidence for an

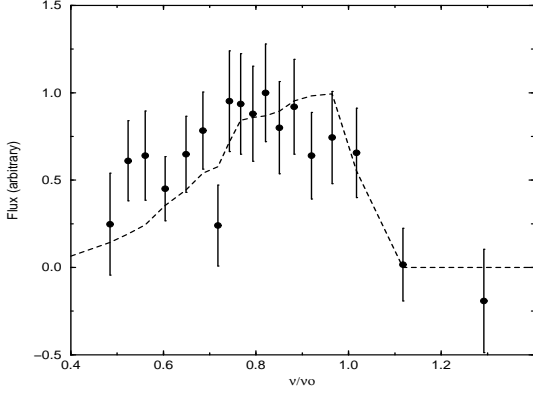


Figure 7. The line shape corresponding to the best-fit values $i = 29^{+2.5}_{-3.2}$, $a_* = 1^{+0}_{-0.01}$ is compared to the data points from Iwasawa et al. (1996). The error bounds on the best fit parameters are 68% confidence intervals obtained by marginalization with a uniform prior over the other parameter.

inclination angle of $\sim 25^\circ$ – 30° and strongly favour an extreme Kerr hole ($a_* > 0.94$) rather than a Schwarzschild hole ($a_* = 0$). The inclination $i \simeq 30^\circ$ arises mainly because of the observed cut-off for energies higher than 6.5 keV, while the observed broad red wing necessitates the high value of a_* . We note that a simple calculation shows that significant line emission below 3.8 keV requires that the disk extend within $1.9r_g$ which in turn requires $a_* > 0.95$.

3.1 Fitting the emissivity profile

The need for an a_* value near 1 is so crucial in obtaining the highly redshifted emission seen in the data, that the observed line can strongly constrain the radial emissivity profile, $\varepsilon(r)$. This is because while a_* near 1 allows a much smaller inner radius of the disk, it is only possible to take advantage of this if we weight the inner regions highly in forming the line profile. This weighting function is of course basically the emissivity profile. We have assumed above the Page & Thorne form, which (for the parameters of interest here) behaves approximately like $r^{-2.8}$ at large r and cuts off to zero at r_{ms} . It is of interest to try to establish quantitatively the $\varepsilon(r)$ profile favoured by the data itself, to see if this can reproduce something like a power law form, or even the cut off at r_{ms} , favoured theoretically. As a first test case, one might attempt to do this with the other important parameters, the inclination angle and the black hole angular momentum parameter, held fixed. At a later stage one could then try to include fitting of all three of i , a_* and a free-format $\varepsilon(r)$ simultaneously. We have written inversion software, incorporating maximum entropy regularization, which can achieve this, and this will be described fully, together with simulations, in a later paper. To show results of immediate interest in relation to MCG-6-30-15, we show in Figs. 8 and 9 the results obtained by this method without any regularization, using just positivity of the emission as the only constraint, and with i and a_* fixed at values plausible on other grounds of 30° and 0.998 respectively. Such an approach is similar to the Lucy algorithm of Manucci, Salvati & Stanga (1992) in application to inverting the profiles of optical Balmer lines, except in the present case

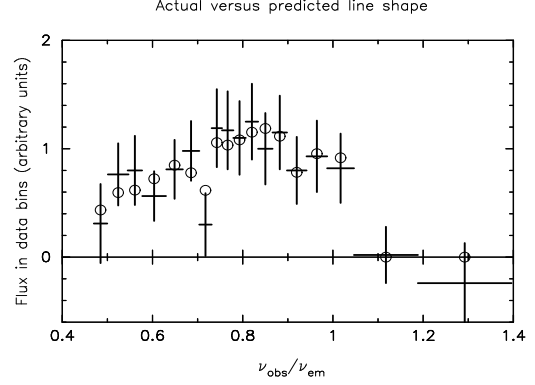


Figure 8. Comparison of actual data points (1 sigma error bars shown) with the results in each bin predicted using the inferred emissivity profile (open circles).

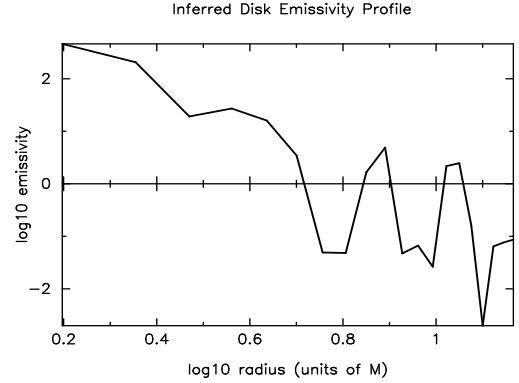


Figure 9. Log-log plot of inferred emissivity profile.

the integral kernel is more complicated and has to be evaluated numerically. Fig 9 shows the inferred emissivity profile as found in 20 radial bins, stretching from r_{ms} to $15r_g$ in r . Some evidence for a power law form is evident, with a slope of perhaps ~ -3.5 , although it obviously becomes noisy at the smaller flux levels. Fig. 8 compares the points predicted using this radial profile (and assuming $i = 30^\circ$ and $a_* = 0.998$) with the observed data. It is evident that a degree of overfitting may be taking place, but that the results look sensible.

4 THE ENHANCEMENT OF EQUIVALENT WIDTH BY RETURNING RADIATION

Light bending effects become very powerful for highly rotating holes and should contribute to enhance the line equivalent width. This bending effect is illustrated in Fig. 10 by a polar diagram showing that for high inclination angles the emission strongly diverges from an isotropic case. The photons released from the inner part of the disk are preferentially bent toward the plane of rotation.

Moreover, a substantial number of the geodesics return to the disk itself — this is the returning radiation first treated by Cunningham (1976). To study the returning radiation, we used the same method of calculation as described in Section 2.1, but placing the observer at a given radius

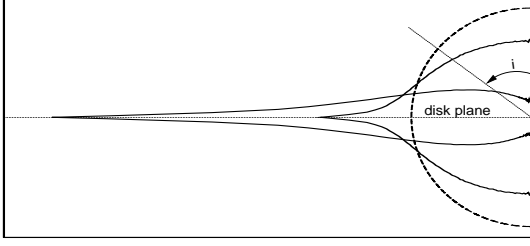


Figure 10. Received power as a function of emitted radius (from left to right: $r = 2r_g$, $r = 8r_g$). The circular curve is for isotropic emission.

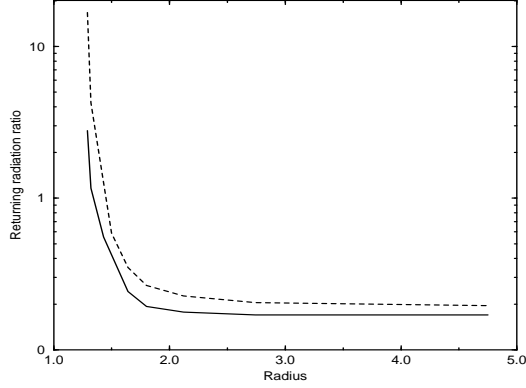


Figure 11. Returning radiation ratio : $F_{ret}(r_{ret})/\epsilon(r_{ret})$ (solid line). The dashed line shows the ratio of returning photons over the number of emitted photons; it is proportional to the enhancement in equivalent width (for a continuum power-law of energy index 1).

r_{ret} on the rotating disk. The result is shown in Fig. 11 as the ratio of returning flux $F_{ret}(r_{ret})$ (coming from any part of the disk) over emitted flux $\epsilon(r_{ret})$ at the same point (assuming again the Page & Thorne law). One can notice that for inner radii (i.e. $r_{ret} < \sim 1.4r_g$) this ratio is larger than unity. Two effects from the returning radiation should be involved in enlarging the equivalent-width of the fluorescent line relative to the primary power-law continuum:

(i) More than half the continuum flux may hit the disk and produce fluorescent photons.

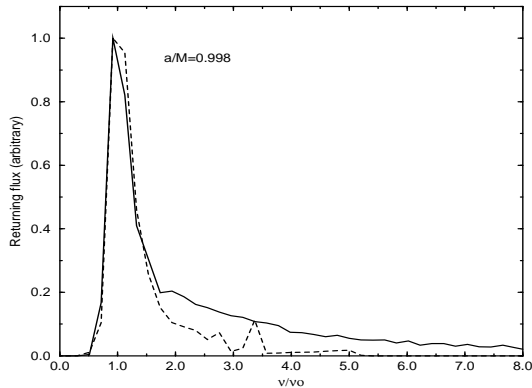


Figure 12. The line profile as seen by an observer rotating with the disk at a radius of $1.5r_g$ (solid line), or $2r_g$ (dashed line).

(ii) Some of the returning photons are strongly blueshifted (Fig. 12). This effect is particularly enhanced on the inner parts of the disk. Then, since the power law slope of the continuum is negative (~ -2), at any given frequency, the continuum flux incident on the disk is higher than the continuum flux which reaches the observer.

Since most of the line emission within $r \sim 1.4r_g$ emerges below 2 keV, the line enhancement due to returning radiation has little effect on the observed profile. An enhancement is instead needed at ~ 4 keV, or from $r \sim 2r_g$, where returning radiation has little effect. Either the geometry of Martocchia & Matt (1996), in which the continuum source does not corotate with the disk, or some other effect (e.g. high ionization of iron in the disk) is needed for the observed increase in line strength (Iwasawa et al. 1996).

More detailed calculations of line strength in both the geometry considered in this paper and that of Martocchia & Matt will be presented in a later paper (Lasenby et al. in preparation). This will cover a wider range of applications, including predicted disk images and some differences from previous results for line profiles from accretion disk will be highlighted.

ACKNOWLEDGEMENTS

ACF thanks the Royal Society for support.

REFERENCES

- Asaoka I., 1989, PASJ, 41, 763
- Bromley B.C., Chen K., Miller W.A., 1997, ApJ, 475, 57
- Cunningham C., 1975, ApJ, 202, 788
- Cunningham C., 1976, ApJ, 208, 534
- Fabian A.C., Rees M.J., Stella L., White N.E., 1989, MNRAS, 238, 729
- Fabian A.C. et al., 1994, PASJ, 46 L59
- Fabian A.C., Nandra K., Reynolds C.S., Brandt W.N., Otani C., Inoue H., Iwasawa K., 1995, MNRAS, 277, L11
- Iwasawa K., Fabian A.C., Mushotzky, Brandt W.N., Awaki H., Kunieda h., 1996, MNRAS, 279, 837
- Iwasawa K. et al., 1996, MNRAS, 282, 1038.
- Kojima Y., 1991, MNRAS, 250, 629
- Laor A., 1991, ApJ, 376, 90
- Luminet J-P., 1979, A&A, 228, 75
- Mannucci F., Salvati M., Stanga R.M., 1992, ApJ, 394, 98
- Martocchia A., Matt G., 1996, MNRAS, 282, L53
- Matsuoka M., Piro L., Yamauchi M., Murakami T., 1990, ApJ, 361, 400
- Mushotzky R.F., Fabian A.C., Iwasawa K., Kunieda H., Matsuoka M., Nandra K., Tanaka Y., 1995, MNRAS, 272, L9
- Nandra K. et al., 1997, ApJ, in press.
- Novikov I.D., Thorne K.S., 1973 in *Black Holes*, ed. C.DeWitte and B.S.DeWitte (Gordon and Breach Science Publishers, New York), p.344
- Page D.N., Thorne K.S., 1974, ApJ, 499, 191
- Pounds K.A., Nandra K., Stewart G.C., George I.M., Fabian A.C., 1990, Nat, 344, 132
- Reynolds C.S., 1997, MNRAS, in press.
- Tanaka Y. et al., 1995, Nat, 375, 659
- Thorne, K.S., 1974, ApJ, 191, 507